



# Dating magmatic and hydrothermal processes using andradite-rich garnet U–Pb geochronometry

Xiao-Dong Deng<sup>1,2</sup> · Jian-Wei Li<sup>1,2</sup> · Tao Luo<sup>1</sup> · Hong-Qiang Wang<sup>2</sup>

Received: 18 March 2017 / Accepted: 6 July 2017 / Published online: 3 August 2017  
© Springer-Verlag GmbH Germany 2017

**Abstract** Andradite-rich garnet is a common U-bearing mineral in a variety of alkalic igneous rocks and skarn deposits, but has been largely neglected as a U–Pb chronometer. In situ laser ablation-inductively coupled plasma mass spectrometry U–Pb dates of andradite-rich garnet from a syenite pluton and two iron skarn deposits in the North China craton demonstrate the suitability and reliability of the mineral in accurately dating magmatic and hydrothermal processes. Two hydrothermal garnets from the iron skarn deposits have homogenous cores and zoned rims ( $\text{Ad}_{86}\text{Gr}_{11}$  to  $\text{Ad}_{98}\text{Gr}_1$ ) with 22–118 ppm U, whereas one magmatic garnet from the syenite is texturally and compositionally homogenous ( $\text{Ad}_{70}\text{Gr}_{22}$  to  $\text{Ad}_{77}\text{Gr}_{14}$ ) and has 0.1–20 ppm U. All three garnets have flat time-resolved signals obtained from depth profile analyses for U, indicating structurally bound U. Uranium is correlated with REE in both magmatic and hydrothermal garnets, indicating that the incorporation of U into the garnet is largely controlled by substitution mechanisms. Two hydrothermal garnets

yielded U–Pb dates of  $129 \pm 2$  ( $2\sigma$ ; MSWD = 0.7) and  $130 \pm 1$  Ma ( $2\sigma$ ; MSWD = 0.5), indistinguishable from zircon U–Pb dates of  $131 \pm 1$  and  $129 \pm 1$  Ma for their respective ore-related intrusions. The magmatic garnet has a U–Pb age of  $389 \pm 3$  Ma ( $2\sigma$ ; MSWD = 0.6), consistent with a U–Pb zircon date of  $388 \pm 2$  Ma for the syenite. The consistency between the garnet and zircon U–Pb dates confirms the reliability and accuracy of garnet U–Pb dating. Given the occurrence of andradite-rich garnet in alkaline and ultramafic magmatic rocks and hydrothermal ore deposits, our results highlight the potential utilization of garnet as a powerful U–Pb geochronometer for dating magmatism and skarn-related mineralization.

**Keywords** Andradite-rich garnet · U–Pb dating · Alkaline magmatism · Skarn · North China craton

## Introduction

Garnet contains variable U coupled with negligible common Pb and has a high closure temperature for the U–Pb isotope system ( $>850$  °C; Mezger et al. 1989), making it a potentially suitable geochronometer for dating high-grade metamorphism (Burton and O’Nions 1992; Vance and Holland 1993; Burton et al. 1995; Jung and Mezger 2003). However, U–Pb dating of low-U (<1 ppm) metamorphic pyrope-almandine garnet is problematic due to the presence of abundant U-rich mineral inclusions, such as uraninite, zircon, monazite, and allanite (DeWolf et al. 1996; Vance et al. 1998; Lima et al. 2012). As such, the garnet U–Pb chronometer has almost been abandoned (Lima et al. 2012), although its potential has long been recognized (Mezger et al. 1989).

Communicated by Franck Poitrasson.

**Electronic supplementary material** The online version of this article (doi:10.1007/s00410-017-1389-2) contains supplementary material, which is available to authorized users.

✉ Xiao-Dong Deng  
dengxiadong@cug.edu.cn

Jian-Wei Li  
jwli@cug.edu.cn

<sup>1</sup> State Key Laboratory of Geological Processes and Mineral Resources, China University of Geosciences, Wuhan 430074, China

<sup>2</sup> Faculty of Earth Resources, China University of Geosciences, Wuhan 430074, China

Grandite garnet is a solid-solution mixture of grossular ( $\text{Ca}_3\text{Al}_2\text{Si}_3\text{O}_{12}$ ) and andradite ( $\text{Ca}_3\text{Fe}_2\text{Si}_3\text{O}_{12}$ ), which often occurs in alkaline and ultramafic intrusions (e.g., Huggins et al. 1977; Barrie 1990; Vuorinen et al. 2005; Scheibner et al. 2007; Python et al. 2007; Smith et al. 2013) and calc-silicate skarns typically associated with economic Fe, Cu, Mo, and W mineralization (e.g., Smith et al. 2004; Meinert et al. 2005; Xu et al. 2016). Thus, dating grandite garnet may potentially provide direct constraints on the time and history of magma emplacement and hydrothermal process (Heaman and LeCheminant 2001; Seman et al. 2017). Grandite garnet can have variable O and Nd initial isotope ratios (Jamtveit and Hervig 1994), which severely complicates its use for Sm–Nd isochron dating. For grandite garnet, the substitution of  $\text{Fe}^{3+}$  for  $\text{Al}^{3+}$  in the octahedral site facilitates incorporation of  $\text{U}^{4+}$  in the dodecahedral site (up to 2700 ppm; Kwak and Abeysinghe 1987; Barrie 1990; Smith et al. 2004; Scheibner et al. 2007), indicating that garnet U–Pb dating can be reliably considered as the age of formation of the mineral. Garnet from magmatic and hydrothermal environments typically contains a variety of mineral inclusions and thus may pose problems for U–Pb geochronological analysis. Such problems, however, can be solved by in situ analytical techniques, such as SIMS (secondary ion mass spectrometry) and LA-ICPMS (laser ablation-inductively coupled plasma mass spectrometry). LA-ICPMS cannot only analyze U and Pb isotopes and trace elements simultaneously (Liu et al. 2010a), but can also mitigate the effects of mineral inclusions in garnet by targeting inclusion-free areas, allowing high-quality data acquisition.

In this paper, we present LA-ICPMS U–Pb isotope and trace element data for the andradite-rich hydrothermal garnets from two iron skarn deposits and magmatic garnets from a syenite intrusion in the North China craton. The aim of our study was to confirm the suitability and reliability of the garnet U–Pb geochronometer in accurately dating certain magmatic and hydrothermal processes.

## Geological setting

The Han-Xing district is located in the central part of the Trans-North China Orogen that separates the North China craton into the Western and Eastern blocks (Fig. 1a). The district is covered by un-metamorphosed Paleozoic marine sedimentary rocks (Fig. 1b), which are intruded by a number of dioritic and monzonitic plutons and stocks (Fig. 1b). Previous zircon U–Pb geochronological studies suggest that the dioritic and monzonitic intrusions were emplaced at  $136 \pm 2$ – $129 \pm 1$  Ma (Li et al. 2013; Deng et al. 2015). Numerous iron skarn deposits commonly occur along the contact zones between the early Cretaceous intrusions and

middle Ordovician carbonate rocks (Fig. 1b). Hydrothermal zircon U–Pb and phlogopite  $^{40}\text{Ar}/^{39}\text{Ar}$  dates for magnetite-bearing skarns reveal that the timing of iron skarn mineralization ranges from  $137 \pm 2$  to  $129 \pm 1$  Ma, which is consistent with the emplacement ages of ore-related intrusions (Deng et al. 2015). Prograde skarns are well-developed in proximal and intermediate zones of the iron skarn deposits throughout the Han-Xing district, and predominantly consist of garnet, diopside, and magnetite. Garnets from the skarns are characterized by andradite-rich grandite, ranging in composition from  $\text{Ad}_{56}\text{Gr}_{43}$  to pure andradite  $\text{Ad}_{100}$  (Zheng 2007; Zhang et al. 2015). Most of the garnet crystals host abundant fluid inclusions with a variety of daughter minerals dominated by halite and sylvite. Fluid inclusions were mostly homogenized to liquid by halite dissolution or vapor disappearance at 380–600 °C and have calculated salinities up to 74% NaCl equiv. (Zheng 2007).

The Chongli district is situated in the northern part of the Trans-North China Orogen (Fig. 1a) and contains more than ten gold deposits hosted in the Devonian Shuiquangou syenite (Bao et al. 2014). The distribution of gold deposits in this district is mainly controlled by the east–west trending faults cutting through the syenite (Fig. 1c). The syenite intruded late Archean to early Paleoproterozoic gneiss, amphibolite and granulite, and was locally covered by early Cretaceous volcanic rocks. Mesozoic granitic intrusions are widespread in the district, including the Triassic Honghualiang ( $235 \pm 2$  Ma) and Guzuizi ( $236 \pm 2$  Ma) syenogranite, and the Cretaceous Shangshuiquan ( $143 \pm 1$  Ma) and Beizaizi ( $131 \pm 2$  Ma) granites (Fig. 1c; Miao et al. 2002; Jiang et al. 2007). The Dongping gold deposit, located in the central part of the Shuiquangou syenite, is the largest gold deposit (>100 t Au) in the Chongli district (Bao et al. 2014). This syenite consists of K-feldspar, albite, hornblende, and aegirine-augite, with accessory andradite-rich garnet, magnetite, zircon, and apatite. The rocks have been altered by post-magmatic hydrothermal fluids, with zircon U–Pb dates ranging from  $352 \pm 3$  to  $394 \pm 3$  Ma (Miao et al. 2002; Bao et al. 2014; Cisse et al. 2017). Multiple stages of hydrothermal alteration have been confirmed by K-feldspar  $^{40}\text{Ar}/^{39}\text{Ar}$  and hydrothermal zircon U–Pb dates at about 360, 240, 170, and 140 Ma (Jiang and Nie 2000; Li et al. 2010; Bao et al. 2014).

## Samples description

Two samples (NMH01 and NMH34) were collected from underground at the Nanminghe iron skarn deposit, which developed along the contact zone between Ordovician dolomitic limestones and an early Cretaceous monzonite pluton in the Han-Xing district. Sample NMH01 was extracted from ore-related monzonite for zircon separation. It is medium-grained, equigranular, and consists

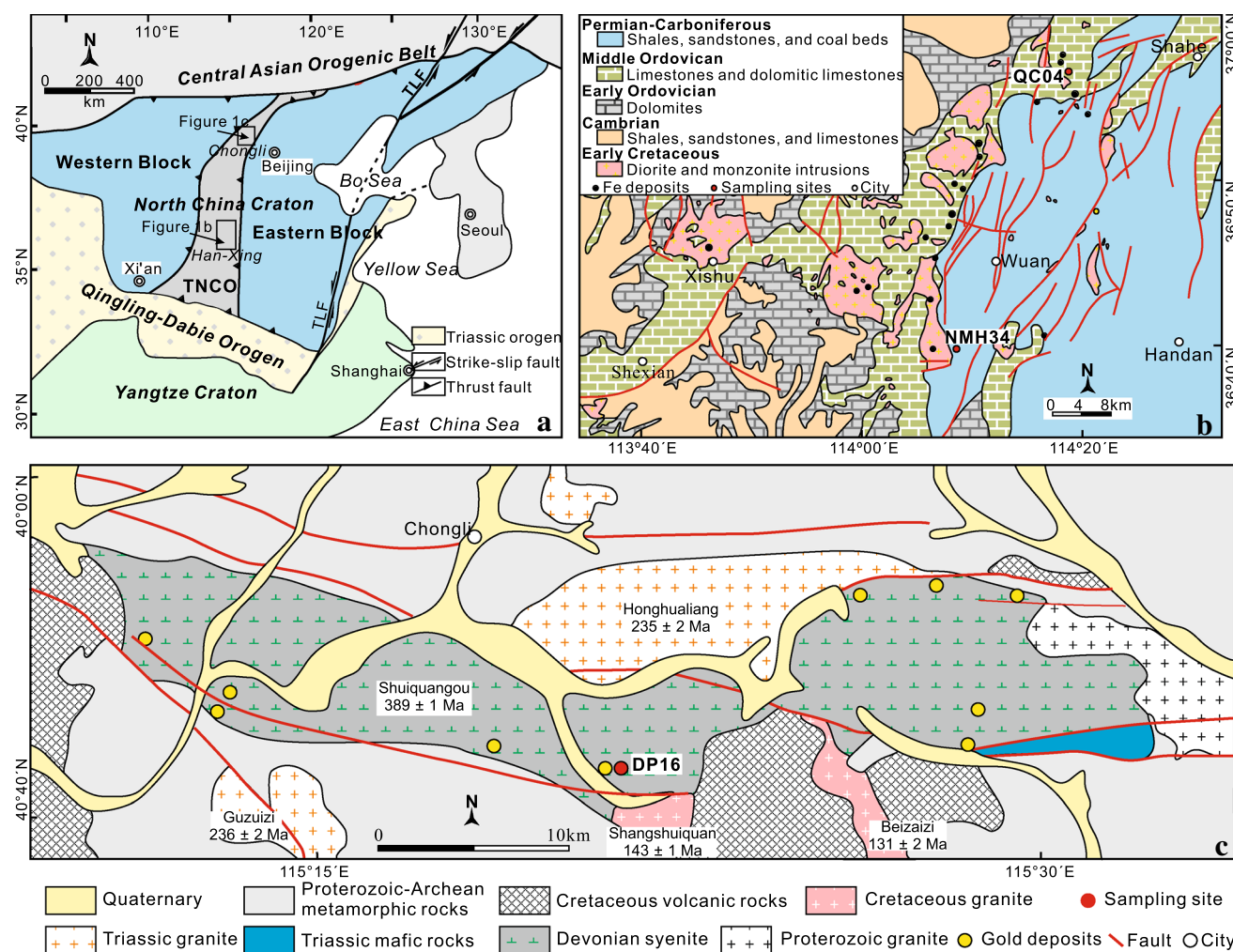


**Fig. 1** **a** A sketch map showing tectonic divisions of the North China craton and the locations of the Han-Xing and Chongli districts (modified from Li et al. 2012). TNCO Trans-North China Orogen, TLF

Tan-Lu Fault. Geological map of the Han-Xing (**b**) and Chongli (**c**) districts showing the sample locations (modified from IGSNC and HGI 1976; Bao et al. 2014)

of K-feldspar (35–40 vol.%), plagioclase (40–50 vol.%), amphibole (10–15 vol.%), and quartz (5 vol.%). Sample NMH34 is a coarse-grained garnet skarn, dominated by garnet (70 vol%) and magnetite (30 vol%). The garnet is commonly enclosed in magnetite and consists of black, euhedral crystals up to 3 cm diameter (Fig. 2a). It has compositionally homogeneous cores and oscillatory zoned rims (Fig. 2b), and commonly contains inclusions of magnetite, hematite, pyrite, quartz, and diopside (Fig. 2c, d).

One sample (QC04) was collected from the Qicun deposit of the Han-Xing district, which is localized along the contact zone between Ordovician limestones and a monzodiorite pluton emplaced at  $129 \pm 1$  Ma (Deng et al. 2015). This sample is a coarse-grained skarn composed of garnet (90 vol%) and magnetite (10 vol%). The garnets are euhedral crystals (0.2–1.0 cm diameter) with red,

blue, and black colors (Fig. 2e). They have compositionally homogeneous cores and oscillatory zoned rims, and commonly contain inclusions of magnetite, hematite, pyrite, quartz, and diopside (Fig. 2f, g).

One garnet-rich syenite sample (DP16) was collected from the Shuiquangou syenite intrusion of the Chongli district. Sample DP16 (Fig. 2h) consists of K-feldspar (65 vol.%), albite (20 vol.%), and hornblende (10 vol.%), with accessory garnet, magnetite, zircon, and apatite. The sample has been variably altered by hydrothermal fluids to form sericite, chlorite, epidote, and clay (Fig. 2i). Garnets typically occur as black crystals, 0.1–0.5 cm in diameter, and are enclosed in K-feldspar and albite (Fig. 2h). They are compositionally homogenous, but may contain inclusions of titanite, K-feldspar, albite, magnetite, and pyrite (Fig. 2j–l).

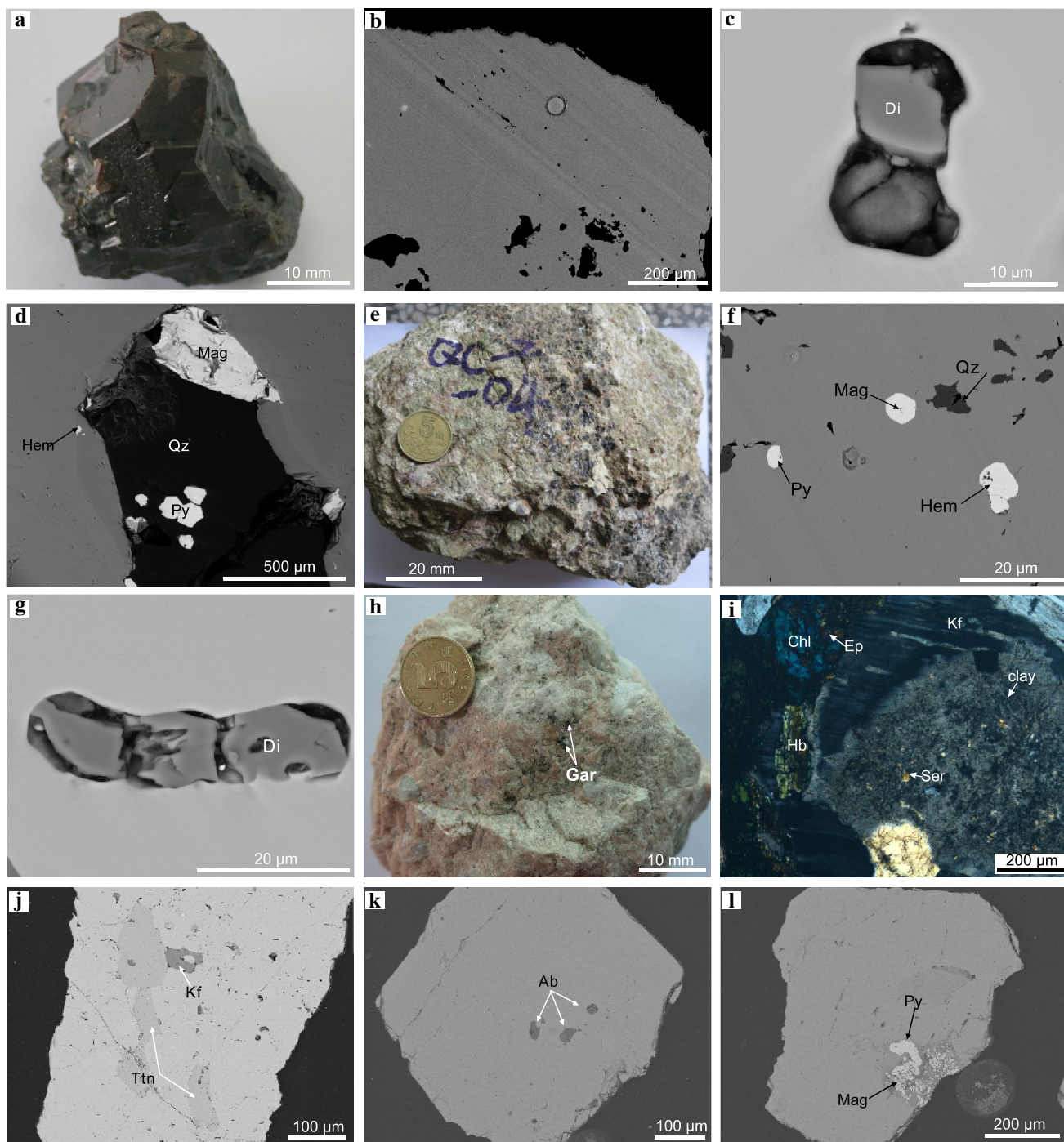


**Fig. 2** Photographs (**a, e, h, i**) and backscattered electron (BSE) images of hydrothermal and magmatic garnets from the North China craton. **a** A ~3 cm garnet crystal from iron mineralized skarn (NMH34) in the Nanminghe deposit, **b** garnet with a homogeneous core and oscillatory zoned rim, **c** diopside and **d** magnetite, hematite, pyrite, and quartz inclusions in garnet crystal of sample NMH34. **e** Hydrothermal garnet (QC04) from the Qicun deposit, **f** diopside, and

**g** magnetite, hematite, pyrite, and quartz in QC04 garnet. **h** Magmatic garnet sample (DP16) from the Dongping syenite pluton, **i** sericite, chlorite, epidote, and clay in sample DP16. **j** K-feldspar and titanite, **k** albite, and **l** magnetite and pyrite inclusions in compositionally homogeneous magmatic garnet. *Ab* Albite, *Chl* chlorite, *Di* diopside, *Ep* epidote, *Gar* garnet, *Hb* hornblende, *Hem* hematite, *Kf* K-feldspar, *Mag* magnetite, *Py* pyrite, *Qz* quartz, *Ser* sericite, *Ttn* titanite

## Analytical methods

Individual crystals of garnet ranging in diameter from 0.1 to 3 cm, were directly hand-picked under a binocular microscope. Zircons were separated using conventional heavy-liquid and magnetic methods and then handpicked under a binocular microscope. All of the garnet and zircon separates were cast in 25 mm epoxy mounts and polished using standard techniques. They were subsequently examined optically and by scanning electron microscopy (SEM) to investigate their internal textures and mineral inclusions. Electron microprobe analyses were performed on a JEOL JXL 8300 Superprobe at the Center for Material Research and Analysis, Wuhan University of Technology. The operating conditions were at 15 kV acceleration voltage, 20 nA beam current, and 5  $\mu\text{m}$  beam diameter. Natural silicate minerals were used as standards, including rhodonite [Mn, Ca], pyrope [Mg, Al, Si], almandine [Fe], and rutile [Ti]. Spectral lines, peak time (s), and off-peak background time (s) used for the WDS analyses were as follows: Si ( $\text{K}\alpha$ , 10, 5), Al ( $\text{K}\alpha$ , 10, 5), Mg ( $\text{K}\alpha$ , 10, 5), Ca ( $\text{K}\alpha$ , 10, 5), Ti ( $\text{K}\alpha$ , 20, 10), Fe ( $\text{K}\alpha$ , 20, 10), Mn ( $\text{K}\alpha$ , 20, 10). Detection limits for the elements are below 0.01 wt % (EMS\_1).

We performed U–Pb isotope and trace element (REE, U, and Th) analyses on the garnet and zircon using an Agilent 7500a ICP-MS instrument equipped with a DUV 193 nm ArF-excimer laser (Geolas 2005, MicroLas Göttingen, Germany) at the State Key Laboratory of Geological Processes and Mineral Resources, China University of Geosciences (Wuhan). The instrumental setups and analytical parameters are listed in EMS\_2. The areas selected for U–Pb dating and trace element analysis were free of inclusions and fractures. The laser beam diameters were set at 32 and 44  $\mu\text{m}$ . A “wire” signal smoothing device is used for laser ablation system, with which smooth signals can be produced even at laser repetition rate of 1 Hz (Hu et al. 2012). Relatively low fluencies and repetition rates (6 J/cm<sup>2</sup> and 5 Hz) were applied to minimize elemental fractionation (El Khorh 2014). Argon was used as make-up gas and mixed with helium as the carrier gas via a T-connector before entering the ICP. Nitrogen (flow rate of 2 ml/min) was added into the central gas flow (Ar + He) of the Ar plasma to decrease the detection limit and improve precision, consequently increasing the sensitivity for most elements by a factor of 2–3 (Hu et al. 2008). The acquisition times for the background and ablation intervals were about 30 and 50 s, respectively. No garnet U–Pb standard was available; thus zircon standard 91500 was used as a standard for mass discrimination and U–Pb isotope fractionation. Preferred U–Pb isotopic ratios used for 91500 are from Wiedenbeck et al. (1995). Time-dependent drifts of U–Th–Pb isotopic ratios were corrected using a linear interpolation (with time) for every five analyses, based on

the variations of 91500 (Liu et al. 2010a). The final uncertainties were propagated from uncertainties of the preferred and measured 91500 values, and the measured sample values (Liu et al. 2010a). Zircon standard GJ-1 was used as the secondary standard for monitoring the precision and accuracy of the U–Pb dating results. The obtained mean  $^{206}\text{Pb}/^{238}\text{U}$  age for GJ-1 is  $601 \pm 2$  Ma ( $2\sigma$ ; MSWD = 0.62;  $n = 39$ ), which is consistent with the recommended values ( $601.95 \pm 0.40$  Ma, Horstwood et al. 2016). Trace elements of garnets were calibrated against the glass standard NIST SRM610, combined with internal standardization (Si). The contents of Si were obtained from electron microprobe analysis. The accuracy and precision were monitored by repeated analyses of BCR-2G, BHVO-2G, and BIR-1G standards (EMS\_3). Off-line selection and integration of background and analyzed signals, time-drift correction, and quantitative calibration for U–Pb isotopes and trace elements analyses were performed using the in-house software *ICPMSDataCal* (Liu et al. 2010b). Concordia diagrams and weighted mean calculations were made using Isoplot/Ex\_ver4.1 (Ludwig 2010).

## Results

### Major and trace elements

Major and trace elements of the garnets are listed in EMS\_1 and 4 and illustrated in Fig. 3. Hydrothermal garnet from sample NMH34 vary in composition from  $\text{Ad}_{94.0}\text{Gr}_{3.6}$  to  $\text{Ad}_{85.6}\text{Gr}_{11.4}$ , with minor spessartine (1.1–2.6%), pyrope (0.1–0.6%), and Ca–Ti garnet (<0.1%) (Fig. 3a). The REE concentrations range from 388 to 2137 ppm (EMS\_4), and chondrite-normalized patterns of the garnet display LREE enrichment and HREE depletion, with positive Eu anomalies ( $\text{Eu/Eu}^* = 2.9\text{--}10.3$ ) (Fig. 3b). Uranium and Th contents range from 20.9 to 107 ppm and 1.38 to 22.9 ppm, respectively, with Th/U ratios of 0.02–0.35 (EMS\_4). Uranium contents of the garnet correlate positively with total REE, including both LREE and HREE contents (Fig. 3d–f).

Hydrothermal garnets from sample QC04 range in composition from  $\text{Ad}_{90.0}\text{Gr}_{7.3}$  to  $\text{Ad}_{98.4}\text{Gr}_{0.7}$ , with minor amounts of spessartine (0.4–0.9%), pyrope (0.5–1.5%), and Ca–Ti garnet (<1.0%) (Fig. 3a). The REE concentrations vary from 264 to 989 ppm (EMS\_4), and chondrite-normalized patterns display LREE enrichment and HREE depletion, with positive Eu anomalies ( $\text{Eu/Eu}^* = 1.0\text{--}21.1$ ) (Fig. 3b). Uranium and Th contents range from 38.3–130 ppm to 0.12–3.03 ppm, respectively, with Th/U ratios of <0.03 (EMS\_4). Uranium contents of these garnets correlate positively with total REE, LREE, and HREE concentrations (Fig. 3d–f).

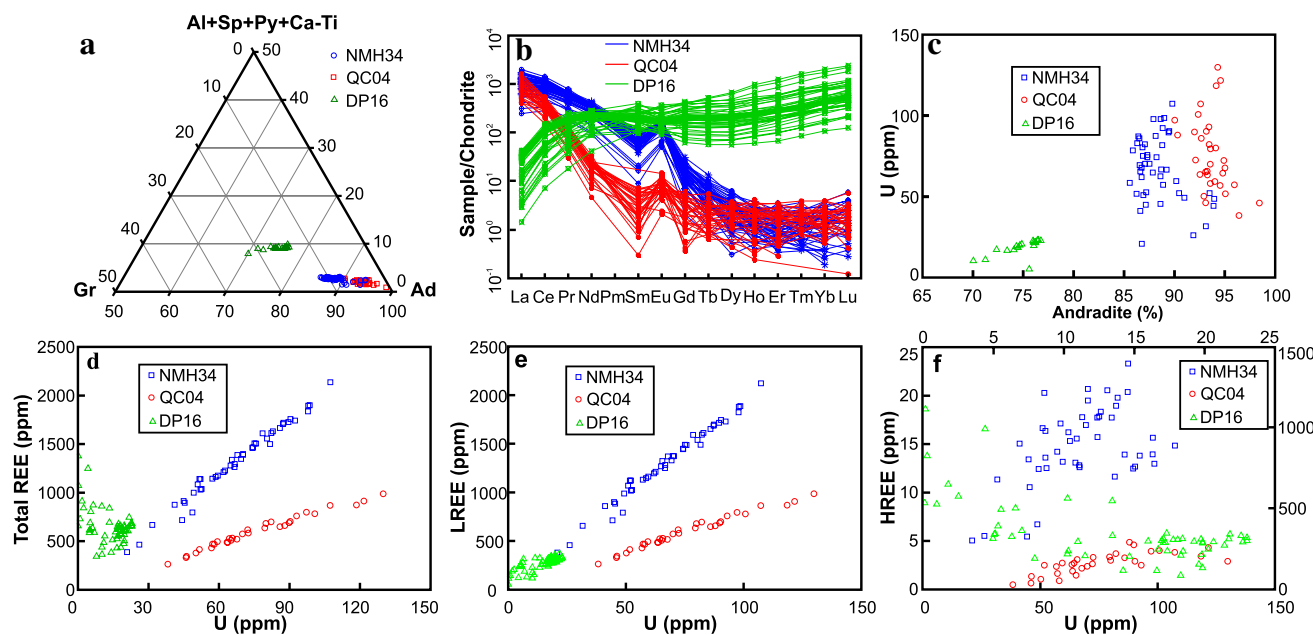


**Fig. 3** Geochemical characteristics of the garnets analyzed in this study. **a** Ternary diagram showing range of garnet components, **b** chondrite-normalized REE patterns, **c** plots of U versus andradite contents, **d** correlation between U and total REE contents, **e** corre-

lation between U and LREE contents, **f** relationship between U and HREE contents. *Ad* Andradite, *Al* almandine, *Ca-Ti* Ca-Ti garnet, *Gr* grossular, *Py* pyrope, *Sp* spessartine

Garnets from sample DP16 range in composition from  $\text{Ad}_{70.1}\text{Gr}_{22.0}$  to  $\text{Ad}_{76.8}\text{Gr}_{14.0}$ , with minor amounts of spessartine (5.0–5.5%), pyrope (0.3–0.5%), and Ca-Ti garnet (2.4–4.4%) (Fig. 3a). They have variable REE contents of 342–1377 ppm (EMS\_4). Chondrite-normalized REE patterns show LREE depletion and HREE enrichment (Fig. 3b), and have weak positive or negative Eu anomalies ( $\text{Eu}/\text{Eu}^* = 0.61\text{--}2.04$ ; EMS\_4). The garnets have variable U (0.11–20.3 ppm) and Th (0.02–6.33 ppm) contents, with Th/U ratios of 0.04–0.33 (EMS\_4). Uranium contents of the garnet correlate positively with andradite components (Fig. 3c) and LREE contents (Fig. 3e), but negatively with HREE concentrations (Fig. 3f).

### U-Pb geochronology

Uranium-lead isotope data of garnet and zircon are listed in EMS\_5 and illustrated as U-Pb concordia diagrams in Fig. 4. Lead isotopic compositions of K-feldspar and pyrite, which are intergrown with the magmatic and hydrothermal garnet, respectively, were used for determining the best common Pb correction (EMS\_6), because of the lack of U and preferential incorporation of Pb in K-feldspar and pyrite.

A total of 46 analyses for sample NMH34 yielded concordant or slightly discordant U-Pb dates and produced a lower intercept  $^{206}\text{Pb}/^{238}\text{U}$  date of  $130 \pm 2$  Ma (Fig. 4a). The  $^{207}\text{Pb}$ -corrected U-Pb dates with 32 and 44  $\mu\text{m}$  spot

sizes yielded mean  $^{206}\text{Pb}/^{238}\text{U}$  dates of  $129 \pm 4$  Ma ( $2\sigma$ ; MSWD = 0.5;  $n = 21$ ) and  $129 \pm 2$  Ma ( $2\sigma$ ; MSWD = 0.7;  $n = 25$ ), respectively (Fig. 4b). The U-Pb dates obtained with a 44- $\mu\text{m}$  beam size have lower analytical uncertainties than those obtained from a 32- $\mu\text{m}$  spot size, because of the increased ion intensity.

Thirty-two analyses for sample QC04 yielded concordant or marginally concordant U-Pb dates and have a lower intercept  $^{206}\text{Pb}/^{238}\text{U}$  date of  $130 \pm 2$  Ma (Fig. 4c). The weighted mean  $^{207}\text{Pb}$ -corrected  $^{206}\text{Pb}/^{238}\text{U}$  age of  $130 \pm 1$  Ma ( $2\sigma$ ; MSWD = 0.5,  $n = 32$ , Fig. 4d) is consistent with the lower intercept  $^{206}\text{Pb}/^{238}\text{U}$  age.

Thirty-eight analyses on magmatic garnet from sample DP16 yielded discordant to concordant U-Pb dates (Fig. 4e). Four analyses were unsuccessful due to extremely low U contents (0.16–0.97 ppm; EMS\_5). The other 34 points have U concentrations of 1.74–20.3 ppm and yielded a lower intercept  $^{206}\text{Pb}/^{238}\text{U}$  date of  $392 \pm 4$  Ma (Fig. 4e) and a weighted mean  $^{207}\text{Pb}$ -corrected  $^{206}\text{Pb}/^{238}\text{U}$  date of  $389 \pm 3$  Ma ( $2\sigma$ , MSWD = 0.6; Fig. 4f).

Zircon from syenite sample (DP-16) in the Dongping deposit can be classified into unaltered and altered. Unaltered zircon usually shows oscillatory zoning in CL images (Fig. 4g), which is characteristic of primary magmatic zircon. Thirteen analyses on 11 unaltered zircon grains yielded concordant U-Pb dates, with a weighted mean  $^{206}\text{Pb}/^{238}\text{U}$  date of  $388 \pm 2$  Ma ( $2\sigma$ ; MSWD = 1.7; Fig. 4h). Altered zircons were characterized by irregular

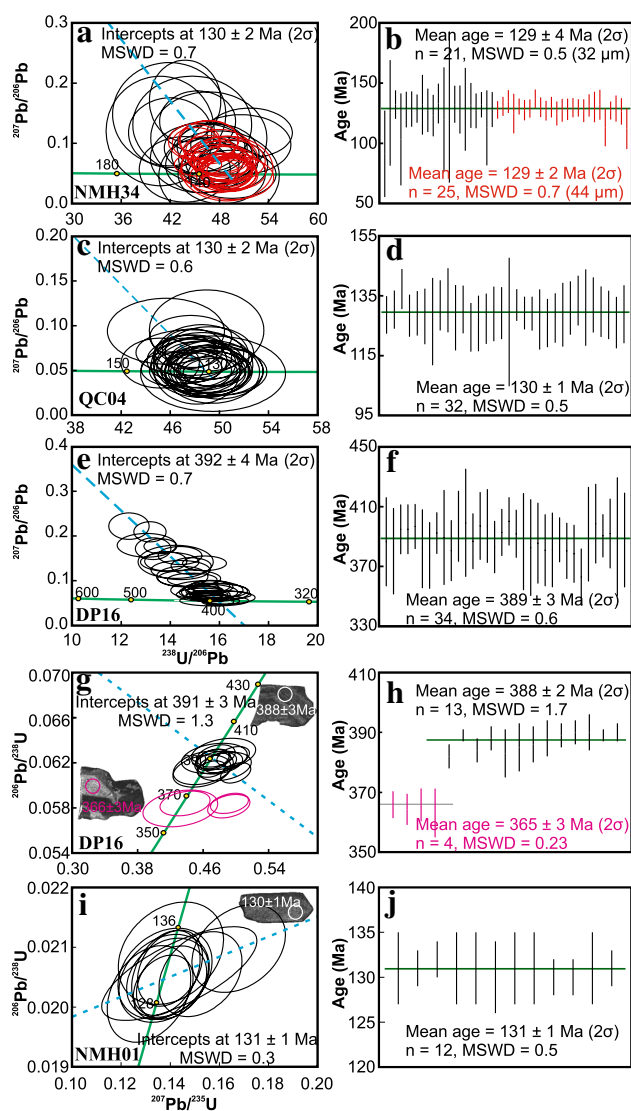


**Fig. 4** Concordia plots and weighted average  $^{207}\text{Pb}$ -corrected  $^{206}\text{Pb}/^{238}\text{U}$  plots of the garnet and zircon analyzed in this study. **a, b** Garnet from the Nanminghe skarn deposit, **c, d** garnet from the Qicun skarn deposit, **e, f** garnet from syenite in the Dongping deposit, **g, h** zircon from the Dongping syenite pluton, and **i, j** zircon from the ore-related monzonite in the Nanminghe deposit. Age uncertainties are quoted as  $2\sigma$ , and individual precision ellipses and error bars are plotted as  $2\sigma$ . MSWD-mean square of weighted deviates

overgrowth zones in CL images (Fig. 4g). Four spots on 4 altered zircon grains yielded concordant and nearly concordant U–Pb dates, ranging in  $^{206}\text{Pb}/^{238}\text{U}$  dates from  $363 \pm 4$  to  $366 \pm 2$  Ma (Fig. 4h).

Twelve analyses on 12 zircon grains from an ore-related monzonite sample (NMH01) in the Nanminghe deposit have U concentrations of 802–4418 ppm, and yielded concordant U–Pb dates (Fig. 4i), which have a weighted mean  $^{206}\text{Pb}/^{238}\text{U}$  date of  $131 \pm 1$  Ma ( $2\sigma$ ; MSWD = 0.5; Fig. 4j).

## Discussion

### Formation of andradite-rich garnet

Garnets from the two iron skarn deposits commonly include magnetite (Fig. 2d, f), which can also enclose garnet or occurs as an interstitial phase between the garnet, suggesting that the two minerals precipitated simultaneously. Hydrothermal garnet also contains minor inclusions of diopside, quartz, and pyrite (Fig. 2c–g), supporting their hydrothermal origin. The garnets are intergrown with hematite, magnetite, and pyrite (Fig. 2d, f), indicating relatively high  $f\text{O}_2$  conditions varying from Mt/Hm to Mt/Py buffers. Fluid inclusion microthermometry has shown that these garnets formed at temperatures of 380–600 °C from saline to hypersaline fluids (Zheng 2007). Oxygen isotope data of hydrothermal garnets from the iron skarn deposits in Han-Xing district indicate  $\delta^{18}\text{O}$  values of the hydrothermal fluids range from 5.3 to 8.5‰ (Zheng 2007), suggesting that these garnets formed from magmatic-dominated fluids. These garnets are characterized by LREE enrichments and HREE depletions, with strong positive Eu anomalies (Fig. 3b). Such REE patterns are commonly interpreted in terms of garnet growth from magmatic-derived fluids under high water/rock ratios (Jamtveit and Hervig 1994; Smith et al. 2004; Gasper et al. 2008; Park et al. 2017).

Garnets from the syenite are typically intergrown with titanite, K-feldspar, and albite (Fig. 2j, k). The magmatic origin of these garnets is supported by their relatively high  $\text{TiO}_2$ -contents of 0.81–1.53 wt% (ESM\_1; Huggins et al. 1977; Scheibner et al. 2007). The garnets are also locally intergrown with magnetite and pyrite (Fig. 2l). These magmatic garnets display LREE depletion and HREE enrichment (Fig. 3b), a feature consistent with formation in a closed system during the early-stage of magmatic crystallization (Scheibner et al. 2007).

### The incorporation of U into andradite-rich garnet

A recognized limitation on U–Pb dating of pyrope–almandine garnet is that the uranium is dominated by the U-rich mineral inclusions, rather than being incorporated into the garnet structure (DeWolf et al. 1996; Vance et al. 1998; Lima et al. 2012). For grandite garnet, however, fission track studies and trace element ratios have shown a homogeneous distribution of U, indicating that the U is hosted within the garnet structure (DeWolf et al. 1996). In this study, the areas selected for garnet U–Pb dating lack visible mineral inclusions as revealed by extensive BSE imaging characterization. The time-resolved signals obtained by depth profile analysis of the observed garnets are flat and stable (Fig. 5), indicating a homogeneous distribution of the U and an absence of inclusions. The obtained U

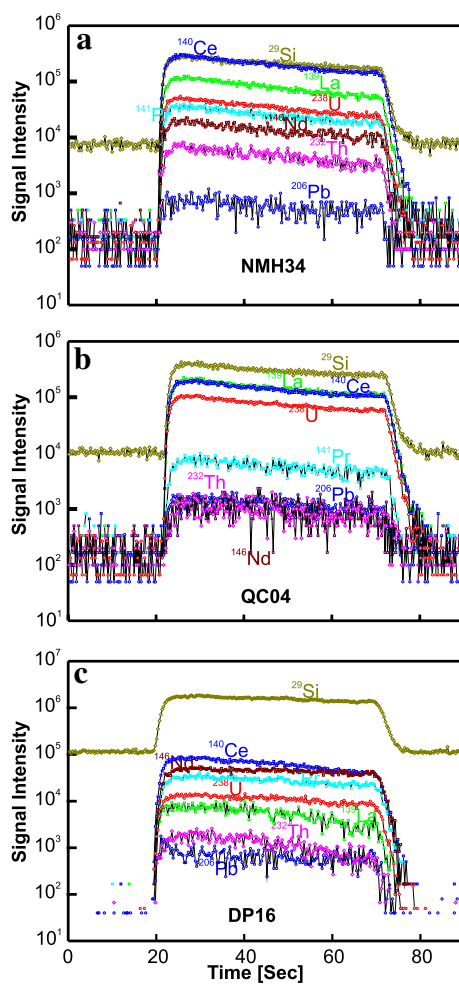


**Fig. 5** Representative time-resolved signals obtained by depth profile analysis of garnets from the Nanninghe (**a**) and Qicun (**b**) iron skarn deposits, and Dongping (**c**) gold deposit, showing flat and stable signals during laser ablation

concentrations correlate well with the contents of andradite (Fig. 3c), indicating that the U is uniformly incorporated in the garnet structure. This view is supported by the observation that the incorporation energy of U in the dodecahedral site significantly decreases with the increase in  $\text{Fe}^{3+}$  cations within the neighboring tetrahedral site (Rák et al. 2011). Collectively, our results strongly suggest that U in all the studied garnets is dominantly structure-bound, thus the U–Pb garnet dates provide direct constraints on the time of garnet growth and, by inference, the emplacement of the syenite intrusion and contact metasomatic formation of the iron skarn deposits.

The incorporation of U into the grandite garnet is possibly controlled by a substitution mechanism (Smith et al. 2004; Gasper et al. 2008). According to ionic radius (Shannon 1976), the incorporation of U into the garnet structure is dominated by the substitution for divalent cations (Ca,

Mg, Mn, or  $\text{Fe}^{2+}$ ) in the dodecahedral position (Smith et al. 2004). The positive correlation between U and REE (Fig. 3d) implies a similar substitution mechanism in grandite garnet (Smith et al. 2004; Gasper et al. 2008; Park et al. 2017). It involves a coupled substitution of  $[\text{U}^{4+}]^{\text{VIII}} + 2[\text{Fe}^{3+}, \text{Al}^{3+}]^{\text{IV}} - [\text{Ca}^{2+}]^{\text{VIII}} + 2[\text{Si}^{4+}]^{\text{IV}}$  (Gasper et al. 2008).

In the eight-fold coordination of garnet, the radius of  $\text{U}^{4+}$  is comparable to those of the HREE (Shannon 1976), and thus a positive correlation is expected between U and HREE. Such a positive correlation is notable for most analyses of the hydrothermal garnet, in contrast to the magmatic garnet in which U is broadly negatively correlated with HREE (Fig. 3f) and positively correlated with LREE (Fig. 3e). The lack of a positive correlation between U and HREE for the magmatic garnet indicates that the incorporation of U into the garnet was not only controlled by substitution mechanisms, but also affected by additional factors. For both hydrothermal garnet samples (NMH34 and QC04), U correlates positively with both LREE and HREE (Fig. 3e, f), indicating that the incorporation of U in the hydrothermal garnet is also dependent on surface sorption during the periods of rapid crystal growth related to the fluid infiltration (Jamtveit and Hervig 1994; Smith et al. 2004). For magmatic garnet (DP16), the negative correlation between U and HREE (Fig. 3f) can be interpreted in terms of co-crystallization of accessory minerals, such as zircon or xenotime (Scheibner et al. 2007).

#### U–Pb isotopic systematics in andradite-rich garnet

Closed U–Pb isotopic systematics are essential for determining the absolute time of garnet formation. The studied syenite, which is the host of the Dongping gold deposit, has undergone multiple stages of hydrothermal alteration, as indicated by the presence of epidote, chlorite, sericite, and clay minerals in the sample (Fig. 2i). Previous K-feldspar  $^{40}\text{Ar}/^{39}\text{Ar}$  and hydrothermal zircon U–Pb dates of the Shuiquangou syenite demonstrated that multiple episodes of hydrothermal alteration occurred at about 360, 260, 180, and 150 Ma (Jiang and Nie 2000; Li et al. 2010; Bao et al. 2014; Cisse et al. 2017). Post-emplacement hydrothermal alteration has also affected the U–Pb isotopic systematics of altered zircon, as confirmed by their younger U–Pb dates (ca. 365 Ma; Fig. 4g, h). Nevertheless, the magmatic garnet yielded coherent U–Pb dates ( $389 \pm 3$  Ma; Fig. 4f) that are perfectly consistent with the U–Pb date of the unaltered magmatic zircons in the same sample ( $388 \pm 2$  Ma; Fig. 4h). This consistency indicates that the U–Pb isotopic systematics in the garnet has remained undisturbed since their formation, confirming the robust nature and reliability of garnet U–Pb geochronometry for accurate dating of magmatic processes.

The iron skarn deposits in the Han-Xing district have also experienced multiple magmatic and hydrothermal events ranging in age from 137 to 125 Ma (Li et al. 2013; Deng et al. 2015). Garnet sample (NMH34) from the Nanminghe deposit has a weighted mean U–Pb date of  $129 \pm 2$  Ma (Fig. 4b), which is the same within uncertainties as a zircon U–Pb date for an ore-related monzonite ( $131 \pm 1$  Ma; Fig. 4j). The weighted mean U–Pb garnet date of  $130 \pm 1$  Ma (Fig. 4d) for sample QC04 from the Qicun deposit is also consistent with zircon U–Pb dates of the ore-related monzodiorite and iron skarn ( $129 \pm 1$  Ma; Deng et al. 2015). The consistency of the U–Pb dates between the garnet and zircon confirms that the garnet remained a closed system since their formation by hydrothermal and magmatic processes.

### Implications for age constraints on magmatic and hydrothermal processes

Zircon may be absent in silica-undersaturated alkaline intrusions, hampering zircon U–Pb dating of such intrusions (e.g., Barrie 1990). Although magmatic zircon is commonly found in silica-saturated alkaline intrusions, it may be incorporated as xenocrystic zircon (e.g., Pidgeon et al. 1996) and/or may tend to be susceptible to isotopic disturbance due to radiation-induced damage (e.g., Soman et al. 2010). These factors may severely limit the use of zircon as a geochronometer for dating alkaline magmatism. Fortunately, magmatic garnet can be present in both silica saturated and undersaturated alkaline magmatic rocks, including ijolite, phonolite, nepheline syenite, syenite, and carbonatite (e.g., Huggins et al. 1977; Vuorinen et al. 2005; Scheibner et al. 2007). The magmatic garnets in alkaline rocks are commonly rich in andradite component and contain several to tens of ppm of U (Scheibner et al. 2007; Rukhlov and Bell 2010) and negligible initial common Pb (e.g., Barrie 1990). These factors make grandite garnet a complementary U–Pb chronometer that can be used in conjunction with zircon U–Pb dating of alkaline magmatism.

Radioisotope dating of ultramafic rocks is important for understanding mantle dynamics and tectonic evolution (Batumike et al. 2008). However, various accessory minerals that can be dated by the U–Pb method (e.g., zircon, baddeleyite, perovskite) are generally absent in ultramafic rocks (Batumike et al. 2008). Fortunately, andradite-rich garnet may crystallize from residual silica melts and fluids during the final stages of crystallization of ultramafic magma (Vuorinen et al. 2005; Dongre et al. 2016). Andradite-rich garnet has been found in ultramafic lamprophyres (Barrie 1990; Tappe et al. 2004), kimberlites (Smith et al. 2013; Dongre et al. 2016), and pyroxenite (Vuorinen et al. 2005). Garnets from ultramafic rocks are commonly enriched in andradite and Ca–Ti garnet components

(Vuorinen et al. 2005; Dongre et al. 2016) and contain several to tens of ppm of U (Barrie 1990). Direct U–Pb dating of andradite-rich garnet thus provides a tool for determining the timing and duration of ultramafic magmatism (Barrie 1990). Andradite-rich garnet may also form at the stage of Ca-metasomatism during serpentinization and hydration of ophiolite complex (Austrheim and Prestvik 2008; Plümper et al. 2014). Thus, garnets in ophiolite complexes provide a potential chronometer for understanding the evolution of oceanic lithosphere.

Direct dating of various hydrothermal activities is essential for better understanding the nature and genesis of economic ore deposits. Grandite garnet is a common primary hydrothermal mineral in a wide variety of ore deposits, such as Fe, Cu, Au, and Mo skarns (e.g., Meinert et al. 2005; Seman et al. 2017), iron-oxide-copper-gold (IOCG) deposits (e.g., Ismail et al. 2014), and REE-U deposits (e.g., Kwak and Abeysinghe 1987; Lentz 1996). The U contents of hydrothermal grandite in such deposits are commonly up to hundreds of ppm (e.g., Kwak and Abeysinghe 1987; Smith et al. 2004; Ismail et al. 2014; Xu et al. 2016). Such high U contents make it possible to date hydrothermal events by in situ U–Pb isotopic analysis.

### Conclusions

We have accurately dated both magmatic garnet from alkaline rocks and hydrothermal garnet from iron skarn deposits using the LA-ICPMS U–Pb geochronometer. Uranium in both the magmatic and hydrothermal andradite-rich garnets shows flat and stable time-resolved depth profiles during measurements with LA-ICPMS and correlates well with the andradite components and rare earth elements' contents therein. This indicates that the U in andradite-rich garnet is dominantly structurally bound. Hydrothermal garnets from the Nanminghe and Qicun iron skarn deposits in the Han-Xing district produce weighted mean U–Pb dates of  $129 \pm 2$  and  $130 \pm 1$  Ma, respectively. These dates are consistent with zircon U–Pb dates of the respective ore-related intrusions ( $131 \pm 1$  and  $129 \pm 1$  Ma). Magmatic garnet from the syenite in the Dongping gold deposit has a weighted mean U–Pb age of  $389 \pm 3$  Ma, which is consistent with the U–Pb date of the unaltered magmatic zircon ( $388 \pm 2$  Ma) from the same sample. The consistency of U–Pb dates between garnet and zircon confirms the suitability and reliability of the garnet U–Pb geochronometer for accurate dating of certain garnet-bearing magmatic rocks and hydrothermal alterations. This consistency of U–Pb dates further indicates that matrix effects between zircon and garnet are not deemed significant in this study. However, it is important to calibrate an accurate and precise garnet standard for U–Pb dating of garnet in the future.

Andradite-rich garnet can occur in ultramafic rocks and ophiolite complexes, and thus may increasingly be used for determining the timing and duration of ultramafic magmatism and ophiolite genesis as well.

**Acknowledgements** We thank Guang Wen, Meijun Yang, and Zhaochu Hu for assistance with the field work, the electron microprobe analyses, and the LA-ICP-MS analyses, respectively. This work was supported by the Ministry of Science and Technology of China (2016YFC0600104), the National Natural Science Foundation of China (41325007, 91514303), and the Research Funds from China University of Geosciences (MSFGPMR03-1, 05; CUG170606). This is contribution 2 from CUG Center for Research in Economic Geology and Exploration Targeting (CREGET). We thank Profs. David Lentz, Paul Robinson, Brent Miller, and Harold Stowell who provided suggestions that have improved the presentation. We also thank the reviewers, Fernando Corfu and an anonymous reviewer, as well as the editor Franck Poitrasson, for their efforts at improving the paper.

## References

- Austrheim H, Prestvik T (2008) Rodingitization and hydration of the oceanic lithosphere as developed in the Leka ophiolite, north-central Norway. *Lithos* 104:177–198
- Bao Z, Sun W, Li C, Zhao Z (2014) U-Pb dating of hydrothermal zircon from the Dongping gold deposit in North China: constraints on the mineralization processes. *Ore Geol Rev* 61:107–119
- Barrie CT (1990) U-Pb garnet and titanite age for the Bristol Township lamprophyre suite, western Abitibi Subprovince, Canada. *Can J Earth Sci* 27:1451–1456
- Batumike JM, Griffin WL, Belousova EA, Pearson NJ, O'Reilly SY, Shee SR (2008) LAM-ICPMS U-Pb dating of kimberlitic perovskite: eocene–oligocene kimberlites from the Kundelungu Plateau, D. R Congo. *Earth Planet Sci Lett* 267:609–619
- Burton KW, O'Nions RK (1992) The timing of mineral growth across a regional metamorphic sequence. *Nature* 357:235–238
- Burton KW, Kohn MJ, Cohen AS, O'Nions RK (1995) The relative diffusion of Pb, Nd, Sr and O in garnet. *Earth Planet Sci Lett* 133:199–211
- Cisse M, Lü X, Algeo TJ, Cao X, Li H, Wei M, Yuan Q, Chen M (2017) Geochronology and geochemical characteristics of the Dongping ore-bearing granite, North China: Sources and implications for its tectonic setting. *Ore Geol Rev*. (in press) doi:10.1016/j.oregeorev.2016.07.006
- Deng X-D, Li J-W, Wen G (2015) U-Pb geochronology of hydrothermal zircons from the Early Cretaceous iron skarn deposits in the Handan–Xingtai District, North China Craton. *Econ Geol* 110:2159–2180
- DeWolf CP, Zeissler CJ, Halliday AN, Mezger K, Essene EJ (1996) The role of inclusions in U-Pb and Sm-Nd garnet geochronology: stepwise dissolution experiments and trace uranium mapping by fission track analysis. *Geochim Cosmochim Acta* 60:121–134
- Dongre AN, Viljoen KS, Rao NVC, Gucsik A (2016) Origin of Ti-rich garnets in the groundmass of Wajrakarur field kimberlites, southern India: insights from EPMA and Raman spectroscopy. *Miner Petrology* 110:295–307
- El Korkh A (2014) Ablation behaviour of allanites during U-Th–Pb dating using a quadrupole ICP-MS coupled to a 193 nm excimer laser. *Chem Geol* 371:46–59
- Gaspar M, Knaack C, Meinert LD, Moretti R (2008) REE in skarn systems: a LA-ICP-MS study of garnets from the Crown Jewel gold deposit. *Geochim Cosmochim Acta* 72:185–205
- Heaman LM, LeCheminant AN (2001) Anomalous U-Pb systematics in mantle-derived baddeleyite xenocrysts from Ile Bizard: evidence for high temperature radon diffusion. *Chem Geol* 172:77–93
- Horstwood MSA, Košler J, Gehrels G, Jackson SE, McLean NM, Paton C, Pearson NJ, Sircombe K, Sylvester P, Vermeesch P, Bowring JF, Condon DJ, Schoene B (2016) Community-derived standards for LA-ICP-MS U-(Th-)Pb geochronology—uncertainty propagation, age interpretation and data reporting. *Geostand Geoanal Res* 40:311–332
- Hu Z, Gao S, Liu Y, Hu S, Chen H, Yuan H (2008) Signal enhancement in laser ablation ICP-MS by addition of nitrogen in the central channel gas. *J Anal At Spectrom* 23:1093–1101
- Hu Z, Liu Y, Gao S, Xiao S, Zhao L, Günther D, Li M, Zhang W, Zong K (2012) A “wire” signal smoothing device for laser ablation inductively coupled plasma mass spectrometry analysis. *Spectrochim Acta Part B* 78:50–57
- Huggins FE, Virgo D, Huckenholz HG (1977) Titanium-containing silicate garnets; II, The crystal chemistry of melanites and schorlomites. *Am Miner* 62:646–665
- IGSNC HGI (Institute of Geological Sciences of North China and Hebei Geological Institute), (1976) Exploration report on the Handan–Xingtai type iron ore deposits in the Taihang Mountain areas. People's Republic of China: Hubei Province, p 154 (in Chinese)
- Ismail R, Ciobanu CL, Cook NJ, Teale GS, Giles D, Mumm AS, Wade B (2014) Rare earths and other trace elements in minerals from skarn assemblages, Hillside iron oxide–copper–gold deposit, Yorke Peninsula, South Australia. *Lithos* 184–187:456–477
- Jamtveit B, Hervig RL (1994) Constraints on transport and kinetics in hydrothermal systems from zoned garnet crystals. *Science* 263:505–508
- Jiang SH, Nie FJ (2000)  $^{40}\text{Ar}/^{39}\text{Ar}$  geochronology study on the alkaline intrusive complex and related gold deposits, north-western Hebei, China. *Geol Rev* 46:621–627 (in Chinese with English abstract)
- Jiang N, Liu Y, Zhou W, Yang J, Zhang S (2007) Derivation of Mesozoic adakitic magmas from ancient lower crust in the North China craton. *Geochim Cosmochim Acta* 71:2591–2608
- Jung S, Mezger K (2003) U-Pb garnet chronometry in high-grade rocks—case studies from the central Damara orogen (Namibia) and implications for the interpretation of Sm-Nd garnet ages and the role of high U-Th inclusions. *Contrib Miner Petrol* 146:382–396
- Kwak TAP, Abeysinghe PB (1987) Rare earth and uranium minerals present daughter crystals in fluid inclusions, Mary Kathleen U-REE skarn, Queensland, Australia. *Miner Mag* 51:665–670
- Lentz DR (1996) U, Mo, and REE mineralization in late-tectonic granitic pegmatites, southwestern Grenville Province, Canada. *Ore Geol Rev* 11:197–227
- Li CM, Deng JF, Chen LH, Su SG, Li HM, Hu SL (2010) Two periods of zircon from Dongping gold deposit in Zhangjiakou-Xuanhua area, northern margin of North China: constraints on metallogenic chronology. *Miner Depos* 29:265–275 (in Chinese with English abstract)
- Li J-W, Bi S-J, Selby D, Chen L, Vasconcelos P, Thiede D, Zhou M-F, Zhao X-F, Li Z-K, Qiu H-L (2012) Giant Mesozoic gold provinces related to the destruction of the North China craton. *Earth Planet Sci Lett* 349:349–350:26–37
- Li S-R, Santosh M, Zhang H-F, Shen J-F, Dong G-C, Wang J-Z, Zhang J-Q (2013) Inhomogeneous lithospheric thinning in the central North China Craton: zircon U-Pb and S-He-Ar isotopic record from magmatism and metallogeny in the Taihang Mountains. *Gondwana Res* 23:141–160

- Lima SM, Corfu F, Neiva AMR, Ramos JMF (2012) U-Pb ID-TIMS dating applied to U-rich inclusions in garnet. *Am Miner* 97:800–806
- Liu Y, Gao S, Hu Z, Gao C, Zong K, Wang D (2010a) Continental and oceanic crust recycling-induced melt–peridotite interactions in the Trans-North China Orogen: U-Pb dating, Hf isotopes and trace elements in zircons from mantle xenoliths. *J Petrol* 51:537–571
- Liu Y, Hu Z, Zong K, Gao C, Gao S, Xu J, Chen H (2010b) Reappraisal and refinement of zircon U-Pb isotope and trace element analyses by LA-ICP-MS. *Chin Sci Bull* 55:1535–1546
- Ludwig K (2010) Isoplot/Ex version 4.1, a geochronological toolkit for Microsoft Ex-cel. Berkeley Geochronology Center Special Publication No. 4
- Meinert LD, Dippe GM, Nicolescu S (2005) World skarn deposits. *Econ Geol* 100(4):299–336
- Mezger K, Hanson GN, Bohlen SR (1989) U-Pb systematics of garnet: dating the growth of garnet in the late Archean Pikwitonei granulite domain at Cauchon and Natawahun Lakes, Manitoba, Canada. *Contrib Miner Petrol* 101:136–148
- Miao L, Qiu Y, McNaughton N, Luo Z, Groves D, Zhai Y, Fan W, Zhai M, Guan K (2002) SHRIMP U-Pb zircon geochronology of granitoids from Dongping area, Hebei Province, China: constraints on tectonic evolution and geodynamic setting for gold metallogeny. *Ore Geol Rev* 19:187–204
- Park C, Song Y, Kang I-M, Shim J, Chung D, Park C-S (2017) Metasomatic changes during periodic fluid flux recorded in granitoid garnet from the Weondong W-skarn deposit, South Korea. *Chem Geol* 451:135–153
- Pidgeon RT, Bosch D, Bruguier O (1996) Inherited zircon and titanite U-Pb systems in an Archaean syenite from southwestern Australia: implications for U-Pb stability of titanite. *Earth Planet Sci Lett* 141:187–198
- Plümper O, Beinlich A, Bach W, Janots E, Austrheim H (2014) Garnets within geode-like serpentinite veins: implications for element transport, hydrogen production and life-supporting environment formation. *Geochim Cosmochim Acta* 141:454–471
- Python M, Ceuleneer G, Ishida Y, Barrat J-A, Arai S (2007) Oman diopside: a new lithology diagnostic of very high temperature hydrothermal circulation in mantle peridotite below oceanic spreading centres. *Earth Planet Sci Lett* 255:289–305
- Rák Z, Ewing RC, Becker U (2011) Role of iron in the incorporation of uranium in ferric garnet matrices. *Phys Rev B* 84:155128
- Rukhlov AS, Bell K (2010) Geochronology of carbonatites from the Canadian and Baltic Shields, and the Canadian Cordillera: clues to mantle evolution. *Miner Petrol* 98:11–54
- Scheibner B, Wörner G, Civetta L, Stosch H-G, Simon K, Kronz A (2007) Rare earth element fractionation in magmatic Ca-rich garnets. *Contrib Miner Petrol* 154:55–74
- Seman S, Stockli DF, McLean NM (2017) U-Pb geochronology of grossular-andradite garnet. *Chem Geol* 460:106–116
- Shannon R (1976) Revised effective ionic radii and systematic studies of interatomic distances in halides and chalcogenides. *Acta Crystallogr Sect A* 32:751–767
- Smith MP, Henderson P, Jeffries TER, Long J, Williams CT (2004) The rare earth elements and uranium in garnets from the Beinn an Dubhaich Aureole, Skye, Scotland, UK: constraints on processes in a dynamic hydrothermal system. *J Petrol* 45:457–484
- Smith CB, Haggerty SE, Chatterjee B, Beard A, Townend R (2013) Kimberlite, lamproite, ultramafic lamprophyre, and carbonatite relationships on the Dharwar Craton, India; an example from the Khaderpet pipe, a diamondiferous ultramafic with associated carbonatite intrusion. *Lithos* 182–183:102–113
- Soman A, Geisler T, Tomaschek F, Grange M, Berndt J (2010) Alteration of crystalline zircon solid solutions: a case study on zircon from an alkaline pegmatite from Zomba-Malosa, Malawi. *Contrib Miner Petrol* 160:909–930
- Tappe S, Jenner GA, Foley SF, Heaman L, Besserer D, Kjarsgaard BA, Ryan B (2004) Torngat ultramafic lamprophyres and their relation to the North Atlantic Alkaline Province. *Lithos* 76:491–518
- Vance D, Holland T (1993) A detailed isotopic and petrological study of a single garnet from the Gassetts Schist, Vermont. *Contrib Miner Petrol* 114:101–118
- Vance D, Meier M, Oberli F (1998) The influence of high U-Th inclusions on the U-Th-Pb systematics of almandine-pyrope garnet: results of a combined bulk dissolution, stepwise-leaching, and SEM study. *Geochim Cosmochim Acta* 62:3527–3540
- Vuorinen JH, Hälenius U, Whitehouse MJ, Mansfeld J, Skelton ADL (2005) Compositional variations (major and trace elements) of clinopyroxene and Ti-andradite from pyroxenite, ijolite and nepheline syenite, Alnö Island, Sweden. *Lithos* 81:55–77
- Wiedenbeck M, Allé P, Corfu F, Griffin WL, Meier M, Oberli F, Quadat AV, Roddick JC, Spiegel W (1995) Three natural zircon standards for U-Th-Pb, Lu-Hf, trace element and REE analyses. *Geostand Newslett* 19:1–23
- Xu J, Ciobanu CL, Cook NJ, Zheng Y, Sun X, Wade BP (2016) Skarn formation and trace elements in garnet and associated minerals from Zhibula copper deposit, Gangdese Belt, southern Tibet. *Lithos* 262:213–231
- Zhang J-Q, Li S-R, Santosh M, Wang J-Z, Li Q (2015) Mineral chemistry of high-Mg diorites and skarn in the Han-Xing Iron deposits of South Taihang Mountains, China: constraints on mineralization process. *Ore Geol Rev* 64:200–214
- Zheng JM (2007) The ore-forming fluid and mineralization of skarn Fe deposits in Handan–Xingtai area, South Hebei [Ph. D Thesis]: China University of Geosciences (Beijing), p 146